Supplementary Information

An ato-Topology Metal-Organic Framework with Large C_2H_2 Adsorption and C_2H_2/CO_2 Separation Capacity

Ting Wang,[‡a] Zhi-Jie Jiang,[‡a] Ying Wang,[a] Rong-Jia Wei,[a] Heng Zeng,*[a] Weigang Lu,*[a] and Dan Li[a]

[a]College of Chemistry and Materials Science, Guangdong Provincial Key Laboratory of Functional Supramolecular Coordination Materials and Applications, Jinan University, Guangzhou 510632, P. R. China.

E-mail: zengheng90@163.com; weiganglu@jnu.edu.cn.

‡These authors contributed equally.

General Methods.

All reagents and solvents were obtained commercially and used as received without further purification. The ligand 5-(3-methyl-5-(pyridin-4-yl)-4*H*-1,2,4-triazol-4-yl)-1,3-benzenedicarboxylic acid (H_2MPTBDC) was purchased from Shanghai Tensus Bio-tech Co., Ltd. Ultrahigh-purity-grade (>99.999 %) N_2, C_2H_2, and CO_2 gases were purchased from Dalian Special Gases CO., Ltd. Mixed gases C_2H_2/CO_2 = 50/50 (mol/mol) was purchased from Huate Gas Co., Ltd.

Syntheses of JNU-7

A mixture of $CoCl_2 \cdot 6H_2O$ (0.02 mmol, 4.78 mg), H_2MPTBDC (0.04 mmol, 12.9 mg), methanol (EtOH, 1.5 mL), and N,N-Dimethylacetamide (DMA, 1.5 mL) were placed in a sealed glass vial (10 mL) and heated at 130 °C for 12 h. After it was cooled to room temperature, the light purple crystals (as-synthesized JNU-7) were collected and washed with DMA three times and exchanged with EtOH three times, then heated under high vacuum at 150 °C for 24 h to afford desolvated JNU-7 (JNU-7a, ~ 8 mg, ~ 65 % yield based on H_2MPTBDC). Anal. calcd. (found) for $C_{16}H_{11}CoN_4O_4 \cdot 5H_2O$: C: 41.03 (40.68%), N: 11.91% (11.86%), H:4.37% (5.49%).

Single-component gas adsorption

At least 100 mg of sample was used for each measurement. JNU-7 was desolvated at 150 °C under dynamic vacuum (below 5 μmHg) for 24 h. Single-component gas adsorption isotherms were measured on an ASAP 2020 PLUS Analyzer (Micromeritics).

Powder X-ray diffraction (PXRD) analysis

Powder x-ray diffraction data was collected using microcrystalline samples on a Rigaku Ultima IV diffractometer (40 kV, 40 mA, Cu Kα, λ = 1.5418 Å). The measurement parameters include a scan speed of 10 (°)/min, a step size of 0.02 (°), and a scan range of 2θ from 5 (°) to 30 (°). For temperature-dependent PXRD, the measurement parameters include a scan speed of 10 °C/min, a step size of 0.02 (°),

and a scan range of 2θ from 5 (°) to 30 (°).

Thermogravimetric analysis (TGA)

Thermogravimetric analysis (TGA) was performed on a TA Instruments Q50 instrument. Measurement was made on approximately 5 mg of dried samples under a N_2 flow with a heating rate of 10 °C/min.

Single-crystal X-ray diffraction analysis

Single crystal diffraction data of as-synthesized JNU-7 (100 K) and JNU-7a (100 K) were collected *via* an Oxford Cryo stream system on a XtaLAB PRO MM007-DW diffractometer system equipped with a RA-Micro7HF-MR-DW (Cu/Mo) X-ray generator and HyPix-6000HE Hybrid Photon Counting (HPC) X-ray detector (Rigaku, Japan, Cu Kα, λ = 1.54178 Å). The structures were solved and refined using Olex 2 with 'XS' and 'XL' plug-ins. For As-synthesized_JNU-7, a solvent mask was calculated, and 168 electrons were found in a volume of 4308 A^3 in 1 void per unit cell. This is consistent with the presence of 1[H_2O] per asymmetric unit, which account for 180 electrons per unit cell. For Desolvated_JNU-7, a solvent mask was calculated and 353 electrons were found in a volume of 9168 A^3 in 1 void per unit cell. This is consistent with the presence of 0.6 EtOH [C_2H_6O] and 0.2 DMF [C_3H_7NO] per asymmetric unit, which account for 454 electrons per unit cell.

The isosteric enthalpy of adsorption (Q_{st})

The isosteric enthalpy of adsorption for C_2H_2 and CO_2 were calculated using the gas adsorption data collected at 273, 283 and 298 K. The adsorption curves were first fitted with the viral equation:[1]

$$\ln P = \ln N + \frac{1}{T}\sum_{i=0}^{m} a_i N^i + \sum_{i=0}^{n} b_i N^i$$

Where N is gas uptake (in mg g^{-1}), P is pressure (in mmHg), a and b are virial coefficients, m and n are the number of coefficients require to adequately describe the isotherm. The parameters that were obtained from the fitting of the C_2H_2 and CO_2

adsorption isotherms can be found in **Fig. S11-12** and **Tables S2**. All isotherms were fitted with $R^2 > 0.999$.

The obtained parameters were used to calculate Q_{st} in the range of adsorption capacity through the virial equation, which is as follows:

$$Q_{st} = -R\sum_{i=0}^{m} a_i N^i$$

IAST calculations of adsorption selectivity

In order to establish the feasibility of C_2H_2/CO_2 separations we performed calculations using the Ideal Adsorbed Solution Theory (IAST) of Myers and Prausnitz.[2]

Let us determine the adsorption selectivity, S_{ads}, defined for separation of a binary mixture of species i and j by

$$S_{ads} = \frac{q_i / q_j}{p_i / p_j}$$

where the q_i represent the molar loadings of component i that is in equilibrium with a bulk gas phase with partial pressures p_i in the mixture.

Column Breakthrough Experiments

The mixed-gas breakthrough separation experiment was conducted under ambient conditions (298 K, 100 kPa) by using a lab-scale fixed-bed system (**Fig. S1**). In a typical breakthrough experiment for C_2H_2/CO_2 (50/50, mol/mol) gas mixture, JNU-7a powder (620 mg) was packed into a stainless steel column (3.15 mm I.D. × 450 mm) with silica wool filling the void space. The sorbent was activated in-situ in the column at 423 K with a high vacuum for 12 h. After the activation process, a helium flow (100 mL min^{-1}) was introduced to purge the adsorbent. The flow of helium was then turned off and a gas mixture of C_2H_2/CO_2 (3 mL min^{-1}) was allowed to flow into the column. Outlet effluent from the column was continuously monitored

using gas chromatography (GC-7890B, Agilent) with a thermal conductivity detector (TCD). After the breakthrough experiment, the sample was regenerated *in-situ* in the column at room temperature with a high vacuum or helium sweeping for 12 h. The complete breakthrough of C_2H_2 was indicated by the downstream gas composition reaching that of the feed gas. On the basis of the mass balance, the gas adsorption capacities can be determined as follows:[3]

$$q_i = \frac{C_i V}{22.4 \times m} \times \int_0^t (1 - \frac{F}{F_0}) dt$$

Where q_i is the equilibrium adsorption capacity of gas i (mmol g^{-1}), C_i is the feed gas concentration, V is the volumetric feed flow rate (mL min^{-1}), t is the adsorption time (min), F_0 and F are the inlet and outlet gas molar flow rates, respectively, and m is the mass of the adsorbent (g).

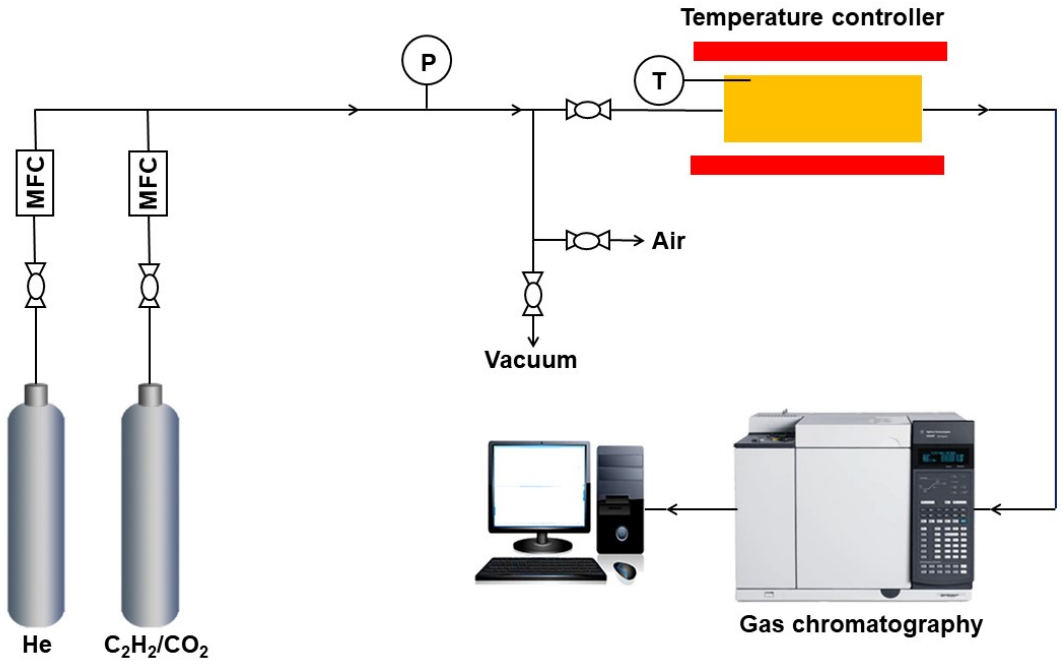

Fig. S1. Schematic illustration of the setup for breakthrough experiments.

Table S1. Crystal data of as-synthesized JNU-7 and desolvated JNU-7.

	as-synthesized JNU-7	**desolvated JNU-7**
Formula	$C_{22}H_{30}CoN_8O_{8.5}$	$C_{18}H_{15.4}CoN_{4.2}O_{4.8}$
Formula weight	559.44	426.27
CCDC number	2205222	2205223
Space group	$R\bar{3}$	$R\bar{3}$
Crystal system	trigonal	trigonal
a (Å)	41.7037(7)	41.862(3)
b (Å)	41.7037(7)	41.862(3)
c (Å)	9.8644(2)	9.5888(5)
α (deg)	90	90
β (deg)	90	90
γ (deg)	120	120
V (Å)^3	14857.7(6)	14553(2)
Z	18	18
ρ calcg/cm^3	1.125	0.876
μ/mm^{-1}	4.464	4.356
R indexes for	R1 = 0.0718	R1 = 0.0597
I>=2σ(I)	wR2 = 0.1962	wR2 = 0.1520
R indexes for	R1 = 0.0847	R1 = 0.0924
all data	wR2 = 0.2053	wR2 = 0.1682
GooF	1.049	0.903
Completeness	99%	96%

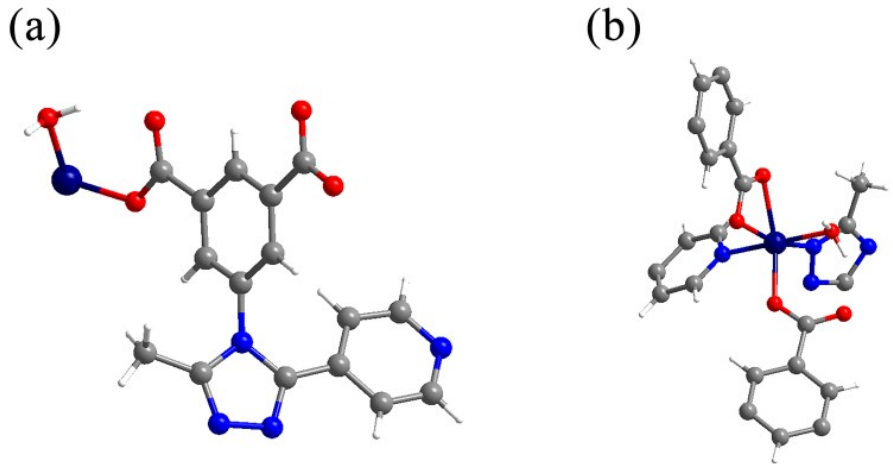

Fig. S1. The asymmetric unit (a) and local coordination environments (b) of JNU-7. (Co, light blue; C, dark grey; N, blue; O, red; H, white).

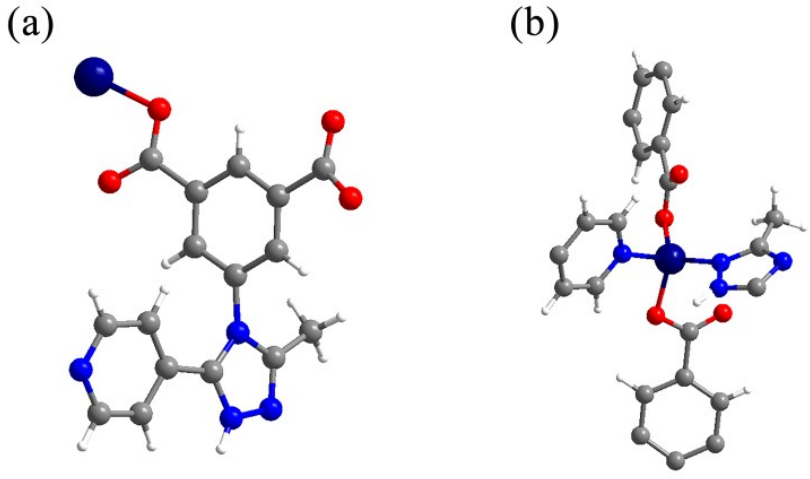

Fig. S2. The asymmetric unit (a) and local coordination environments (b) of JNU-7a. (Co, light blue; C, dark grey; N, blue; O, red; H, white).

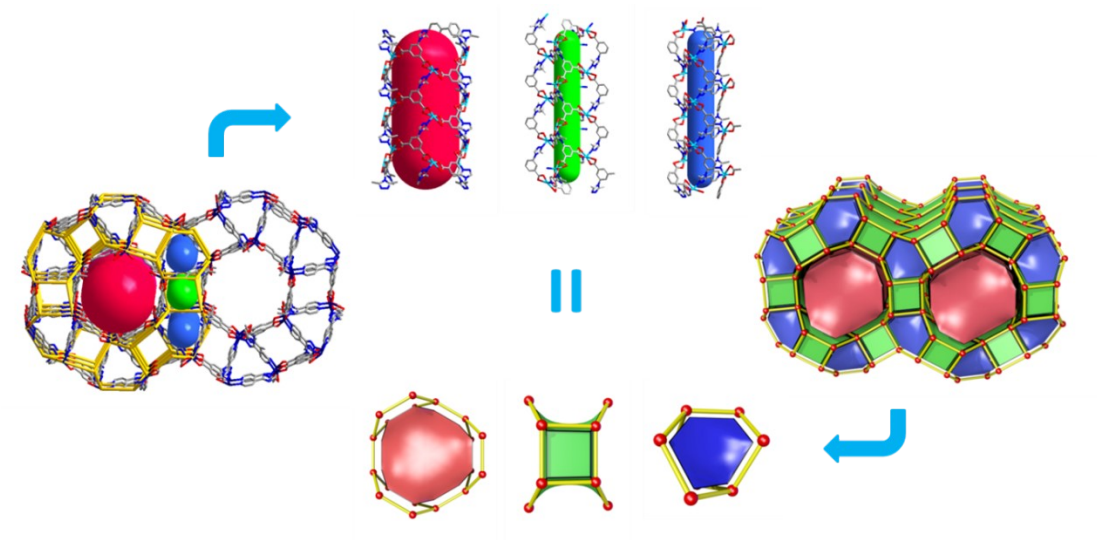

Fig. S3. One-dimensional channels in a three-dimensional structure and corresponds to the tiles in a topological structure.

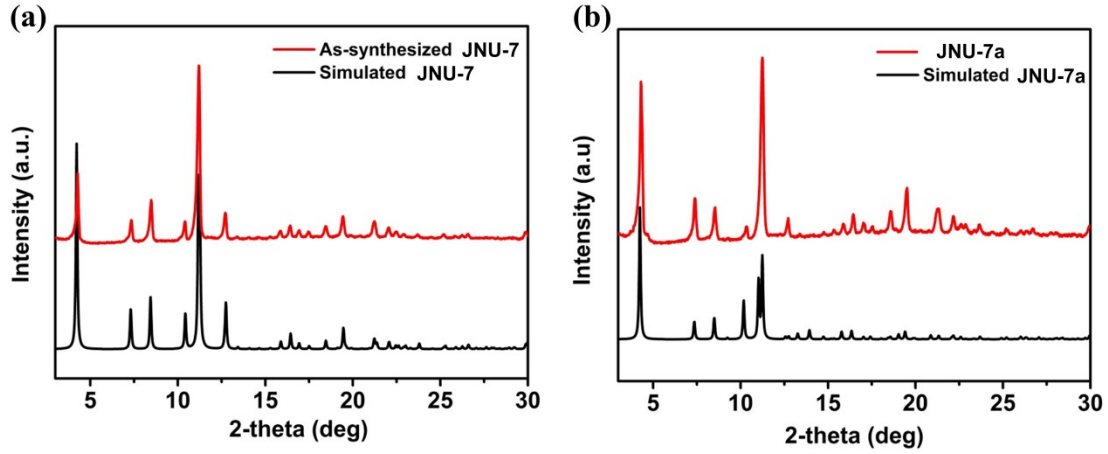

Fig. S4. PXRD patterns of JNU-7 (a) and JNU-7a (b), simulated (black) and as-synthesized (red).

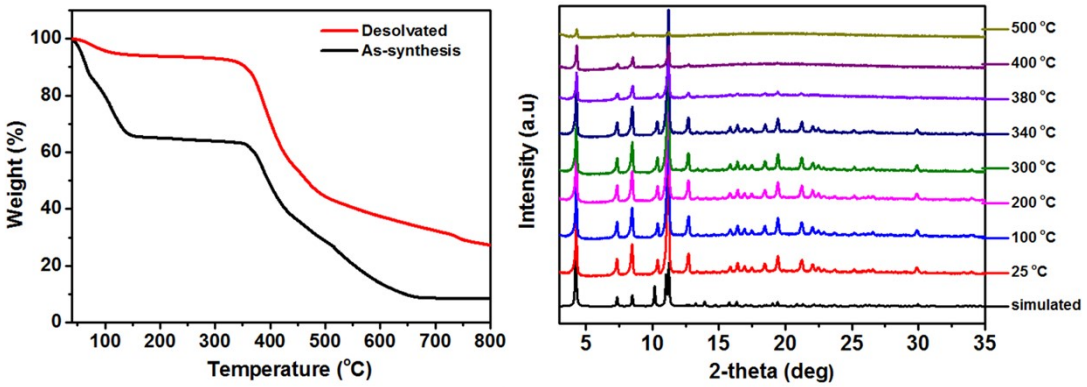

Fig. S5. (a) Thermogravimetric analysis (TGA) curve of the JNU-7 (black) and JNU-7a (red). (b) *In-situ* variable-temperature PXRD (VT-PXRD) patterns of JNU-7a under a N_2 atmosphere.

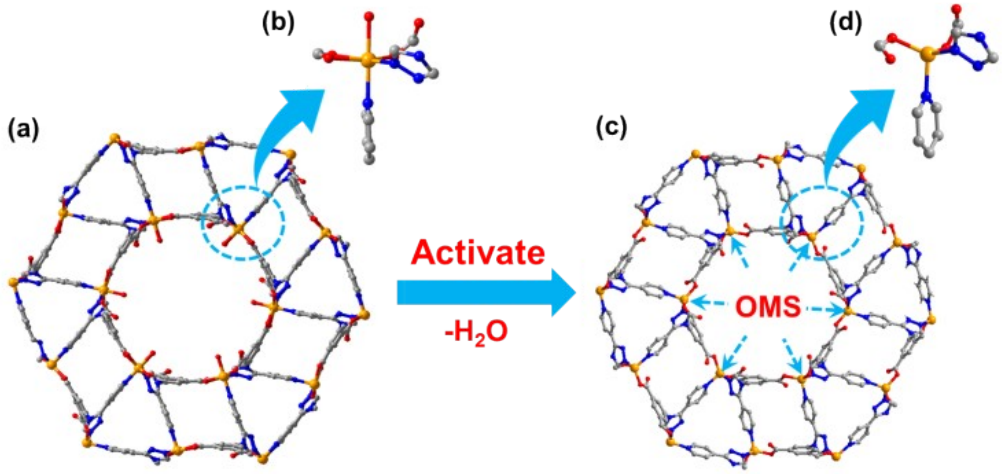

Fig. S6. Analysis of the structural transformation and the formation of open metal sites. The crystal structure of JNU-7 (a) and its metal coordination environment (b) seen in the c direction. The crystal structure of JNU-7a (c) and its metal coordination environment (d) seen in the c direction.

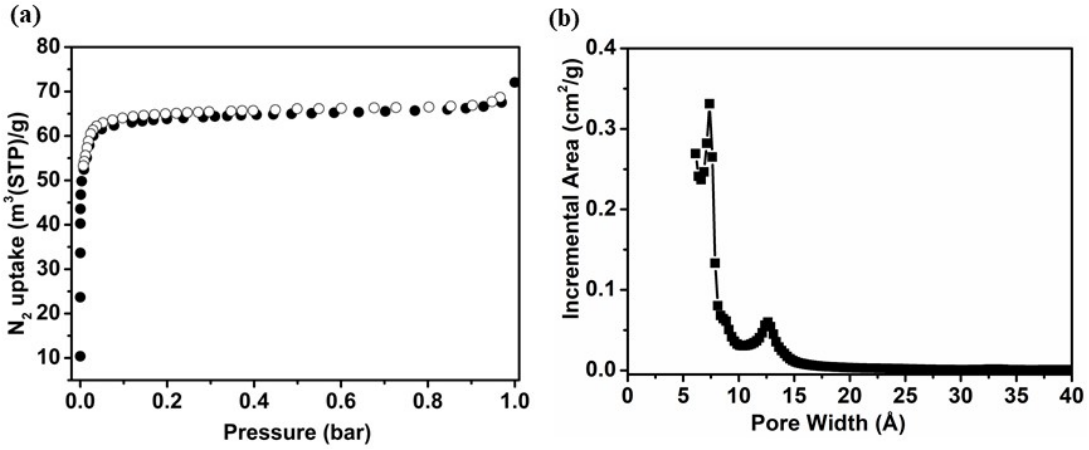

Fig. S7. (a) N_2 adsorption/desorption isotherms of JNU-7 (activated at RT) at 77 K. (b) calculated pore-size distribution based on the adsorption branch, the solid ball is adsorption and the hollow ball is desorption.

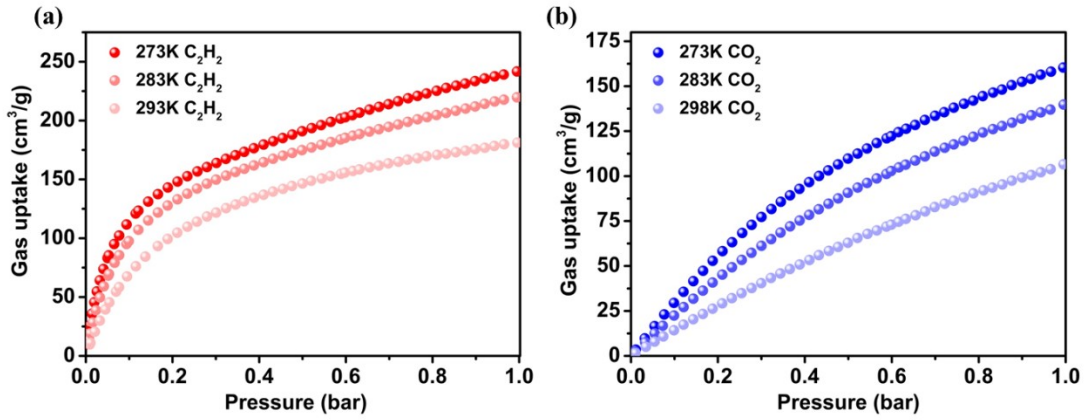

Fig. S8. C_2H_2 and CO_2 adsorption isotherms of JNU-7a at different temperatures.

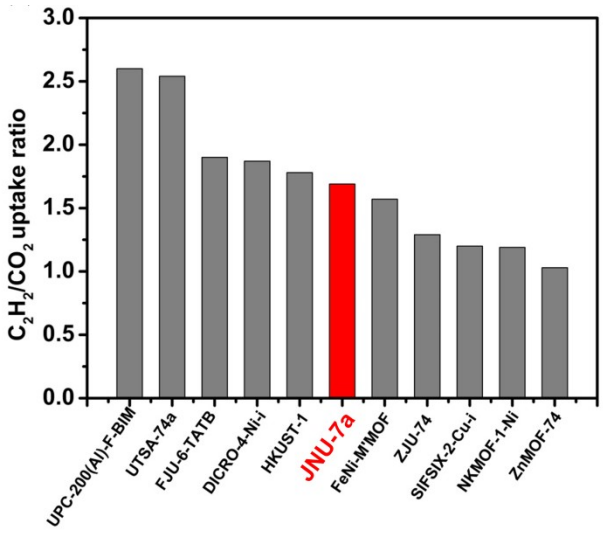

Fig. S9. Comparison of C_2H_2/CO_2 uptake ratio among representative MOFs for C_2H_2/CO_2 separation.

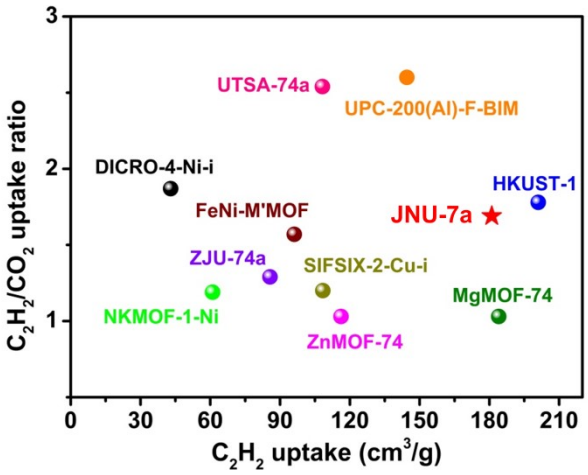

Fig. S10. C_2H_2/CO_2 uptake ratio as a function of C_2H_2 uptakes for JNU-7a and other select separating C_2H_2 MOFs.

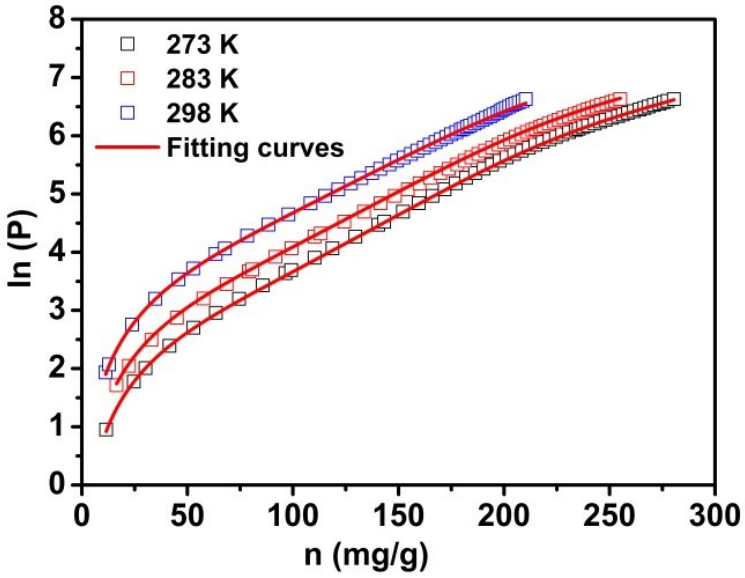

Fig. S11. Virial equation fitting of the C_2H_2 adsorption isotherm of JNU-7a at 273, 283 and 298 K.

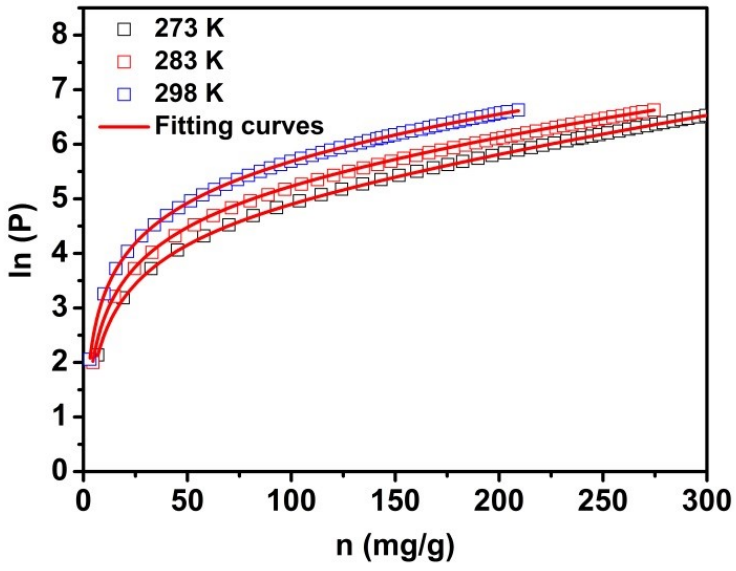

Fig. S12. Virial equation fitting of the CO_2 adsorption isotherm of JNU-7a at 273, 283 and 298 K.

Table S2. Isosteric heats of adsorption of C_2H_2 and CO_2 fitting parameters for JNU-7a.

Parameter	C_2H_2	CO_2
a_0	-3255.57667	-2374.14711
a_1	-1.40753	-3.17967
a_2	-0.0195	0.00976
a_3	4.51322E-4	5.2737E-5
a_4	-1.69532E-6	-1.64708E-7
a_5	2.10301E-9	1.80325E-10
R^2	0.999	0.999

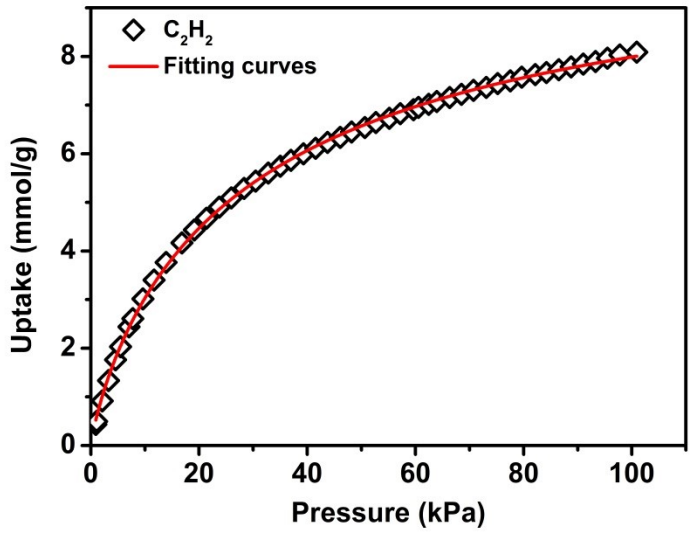

Fig. S13. Single-site Langmuir-Freundlich fitting of the C_2H_2 adsorption isotherm of JNU-7a at 298 K.

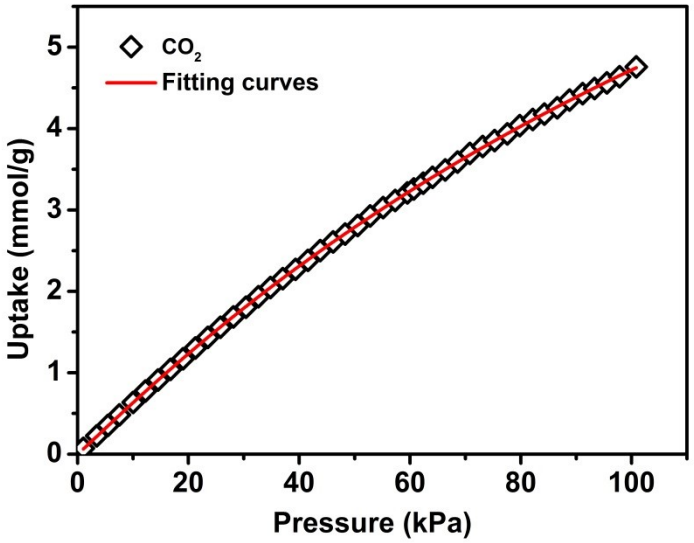

Fig. S14. Single-site Langmuir-Freundlich fitting of the CO_2 adsorption isotherm of JNU-7a at 298 K.

Theoretical Calculations

To better study the adsorption and separation mechanism, Grand Canonical Monte Carlo (GCMC) simulations were performed by RASPA2 software[4,5]. The single-component adsorption isotherms of C_2H_2 and CO_2 on JNU-7a were simulated at 298 K and pressure up to 1 bar. The Lennard-Jones (LJ) parameters of JNU-7a were taken from the universal force field (UFF),[6] whereas C_2H_2 and CO_2 molecules were obtained from literatures.[7,8] The LJ parameters of different atom types were computed using the Lorentz-Berthelot mixing rules. The cut-off radius was chosen as 14 Å for the LJ potential, and the long-range electrostatic interactions were handled using Ewald summation technique. The equilibration steps and production steps were both set as 1.0×10^7. The DDEC charges[9] of the framework atoms were calculated by the Vienna ab initio simulation package (VASP)[10,11]. Perdew-Burke-Ernzerhof (PBE) functional with generalized gradient approximation (GGA) was used to evaluate the electron exchange correlation.

To better explain the host-guest interactions between JNU-7a and gas molecules, the dispersion-corrected density functional theory (DFT-D) calculations were performed using Gaussian 16 software.[12] The cluster models were extracted from the JNU-7a framework, and the truncated bonds were saturated by hydrogen atoms or methyl groups. All geometry optimizations were performed at the B3LYP-D3(BJ)/6-31G* level for the non-metal atoms.[13-15] For Co atom, the LanL2DZ basis set[16] was used to take into account the relativistic effects. Frequency analyses were performed at the same computational level to confirm local minima for each optimized structure. Based on the optimized geometries, these binding energies (ΔE) were corrected from the basis set superposition error (BSSE) by the counterpoise procedure.[17] The binding energy (ΔE) of gas molecules adsorbed in JNU-7a was calculated with the following equation:

$$\Delta E = E_{gas@JNU-7a} - E_{JNU-7a} - E_{gas} + E_{BSSE}$$

Where $E_{gas@JNU-7a}$, E_{JNU-7a}, E_{gas} are the optimization energy of JNU-7a with an adsorbed gas molecule, JNU-7a structure and isolated gas molecule, respectively. while the E_{BSSE} can correct for weak intermolecular interactions.

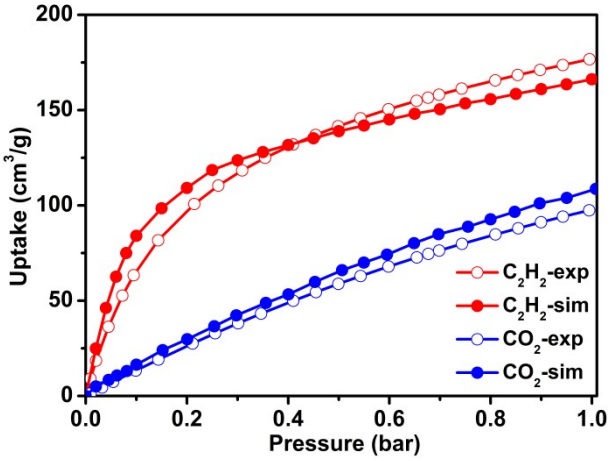

Fig. S15. Experimental and simulated adsorption isotherms of C_2H_2 (red) and CO_2 (blue) at 298 K and up to 1 bar.

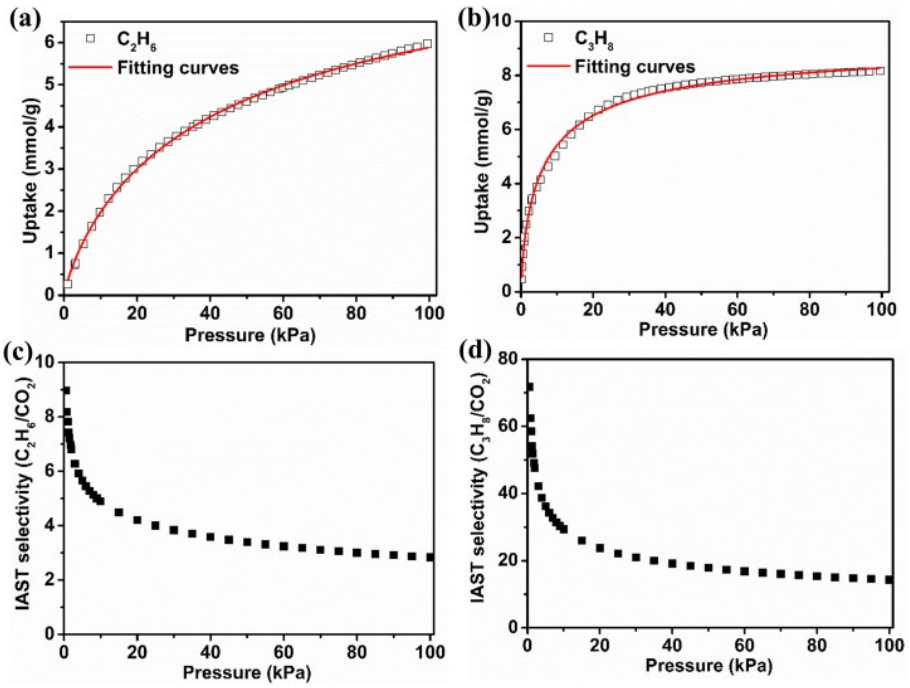

Fig. S16. Single-site Langmuir-Freundlich fitting of the (a) C_2H_6 and (b) C_3H_8 adsorption isotherm of JNU-7a at 298 K. (c) IAST selectivity of JNU-7a for C_2H_6/CO_2 (v/v, 50:50) mixture. (d) IAST selectivity of JNU-7a for C_3H_8/CO_2 (v/v, 50:50) mixture.

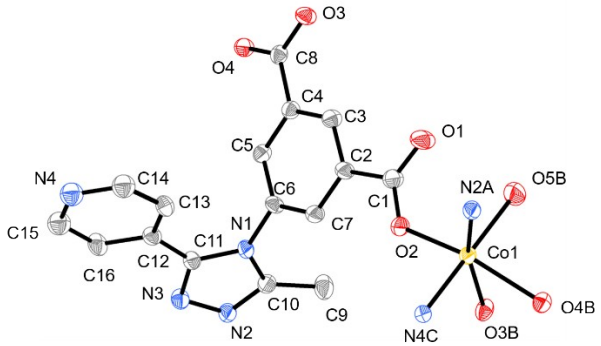

Fig. S17. ORTEP diagram of As-synthesized_JNU-7 at 100 K with 50% thermal ellipsoid probability. Solvent molecules and hydrogen atoms are omitted for clarity. Symmetry operation: A (x, y, 1+z); B (2/3+x-y, 1/3+x, 4/3-z); C (1/3-x+y, 2/3-x, 2/3+z).

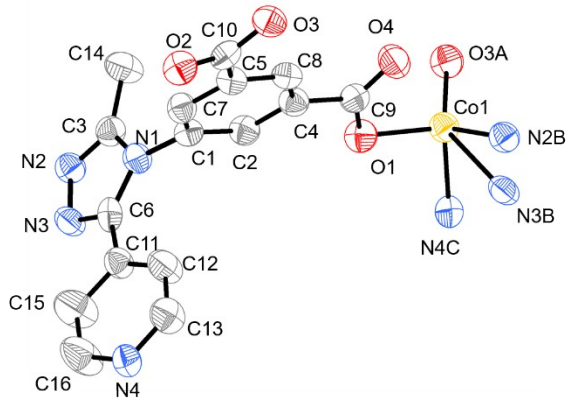

Fig. S18. ORTEP diagram of Desolvated_JNU-7at 100 K with 50% thermal ellipsoid probability. Solvent molecules and hydrogen atoms are omitted for clarity. Symmetry operation: A (1/3+y, 2/3-x+y, 2/3-z); B (x, y, -1+z); C (2/3-y, 1/3+x-y, -2/3+z).

Table S3. Langmuir-Freundlich parameters from the fitting of C_2H_2 and CO_2 adsorption isotherms of JNU-7a at 298 K. The R^2 values are also provided.

Parameter	C_2H_2	CO_2
$q_{A,sat}$	10.92482	14.00029
b_A	0.05419	0.00439
n_A	0.85041	1.03206
R^2	0.999	0.9999

Table S4. Comparison of the C_2H_2 adsorption uptake, C_2H_2/CO_2 selectivity, and heat of adsorption data in JNU-7a with some top-performing C_2H_2-selective materials reported.

Materials	**S_ABET (m^2/g)**	**Gas uptake (298 K)**		**C_2H_2/CO_2**	**Q_{st} of C_2H_2 (kJ/mol)**	**IAST**	**Ref.**
		C_2H_2	**CO_2**				
JNU-7a	**2046**	**176**	**97**	**1.8**	**27**	**12-5**	This work
NKMOF-1-Ni	380	61	51.1	1.19	58.0	249.3-30	18
UTSA-74a	830	108.2	70.9	2.54	32	20-9	19
CoMOF-74	1056	197	-	-	50.1	-	20
MgMOF-74	1495	184	179	1.03	34	1.03	21
HKUST-1	1401	201	113	1.78	39	11	22
DICRO-4-Ni-i	398	43	23	1.87	37.7	18.2-13.9	23
HOF-3a	165	47	21	2.24	19	14	24
UTSA-300a	311	68.9	3.3	20.9	57.6	0.02-743	25
FeNi-M'MOF	383	96.1	60.9	1.57	27–32.8	24	26
UPC-200(Al)-F-BIM	-	144.5	55.5	2.6	18.9-20.5	3.1	27
FJU-6-TATB	1306	110	58	1.9	-	5.3-3.1	28
JNU-1	818	64	–	6.68	13-47.6	285.6-6.6	29
ZJU-74	694	85.7	66.3	1.29	45-65	170-36.5	30
ATC-Cu	600	112.2	90.05	1.25	79.1	53.6	31

Table S5. Contributions of open metal sites (OMSs) and pore space in acetylene uptakes for selected MOFs at room temperature and 100 kPa for volumetric capacity in the unit of cm^3 (STP) cm^3.

Materials	Framework Density (g/cm^3)	OMS density ($mmol/cm^3$)	C_2H_2 uptake (cm^3/cm^3)			Ref.
			By OMS	By pore space	Sum	
JNU-7	**0.785**	**2.05**	**46**	**112**	**158**	This work
HKUST-1	0.879	4.36	97	80	177	22
CoMOF-74	1.169	7.49	168	62	230	20
MgMOF-74	0.909	7.49	199	-	184	21
ZJU-5	0.598	2.31	52	63	115	32
NOTT-101	0.684	2.35	53	73	126	33
FJI-H8	0.873	3.13	70	126	196	34
UTSA-74a	1.342	8.3	186	-	145	19
FeNiM'MOF	1.375	9.2	206	-	133	26
ZJU-74	1.353	9.1	204	-	116	30

Table S6. Breakthrough calculations for separation of 50/50 C_2H_2/CO_2 mixture at 298 K.

	C_2H_2 adsorbed during 0-τ_{break} mol L^{-1}	**Ref.**
JNU-7a	4.44	This work
UTSA-74a	4.86	19
PCP-33	4.16	35
HOF-3	0.7	36

Refrence

1. M. Dinca, A. Dailly, Y. Liu, C. M. Brown, D. A. Neumann and J. R. Long, J. Am. Chem. Soc., 2006, **128**, 16876-16883.

2. A. L. Myers and J. M. Prausnitz, AlChE J., 1965, **11**, 121-127.

3. J. Liu, J. Tian, P. K. Thallapally and B. P. McGrail, The Journal of Physical Chemistry C, 2012, **116**, 9575-9581.

4. D. Dubbeldam, A. Torres-Knoop, K. S. Walton, *Mol. Simul.* 2013, **39**, 1253−1292.

5. D. Dubbeldam, S. Calero, D. E. Ellis, R. Q. Snurr, Nanoporous Materials. *Mol. Simul.* 2016, **42**, 81−101.

6. A. K. Rappé, C. J. Casewit, K. S. Colwell, W. A. Goddard, W. M. Skiff, UFF, *J. Am. Chem. Soc.* 1992, **114**, 10024−10035.

7. W. L. Jorgensen, J. D. Madura, C. J. Swenson, *J. Am. Chem. Soc.* 1984, **106**, 6638−6646.

8. A. Garcia-Sanchez, C. O. Ania, J. B. Parra, D. Dubbeldam, T. J. H. Vlugt, R. Krishna, Calero, S. *J. Phys. Chem. C* 2009, **113**, 8814−8820.

9. T. A. Manz, D. S. Sholl, *J. Chem. Theory Comput.* 2010, **6**, 2455−2468.

10. G. Kresse, J. Furthmuller, *Phys. Rev. B: Condens. Matter Mater. Phys.* 1996, **54**, 11169−11186.

11. G. Kresse, D. Joubert, *Phys. Rev. B: Condens. Matter Mater. Phys.* 1999, **59**, 1758−1775.

12. M. J. Frisch, G. W. Trucks, H. B. Schlegel, G. E. Scuseria, M. A. Robb, J. R. Cheeseman, G.Scalmani, V. Barone, G. A. Petersson, H. Nakatsuji, Gaussian 16, revision B.01; Gaussian, Inc.: Wallingford, CT, 2016. **66**.

13. A. D. Becke, *J. Chem. Phys.* 1992, **96**, 2155−2160.

14. S. Grimme, J. Antony, S. Ehrlich, H.Krieg, *J. Chem. Phys.* 2010, **132**, 154104

15. P. C. Hariharan, J. A. Pople, *Theoretica Chimica Acta* 1973, **28**, 213−222.

16. L. E. Roy, P. J. Hay, R. L. Martin, *J. Chem. Theory Comput.* 2008, **4**, 1029−1031.

17. S. F. Boys, F. Bernardi, *Mol. Phys.* 1970, **19**, 553−566.

18. Y. L. Peng, T. Pham, P. Li, T. Wang, Y. Chen, K. J. Chen, K. A. Forrest, B. Space, P. Cheng, M. J. Zaworotko and Z. Zhang, *Angew. Chem. Int. Ed*., 2018, **57**, 10971−10975.

19. F. Luo, C. Yan, L. Dang, R. Krishna, W. Zhou, H. Wu, X. Dong, Y. Han, T. L. Hu, M. O'Keeffe, L. Wang, M. Luo, R. B. Lin and B. Chen, *J. Am. Chem. Soc*., 2016, **138**, 5678−5684.

20. S. Xiang, W. Zhou, Z. Zhang, M. A. Green, Y. Liu and B. Chen, *Angew. Chem. Int. Ed*., 2010, **122**, 4719−4722.

21. E. D. Bloch, W. L. Queen, R. Krishna, J. M. Zadrozny, C. M. Brown and J. R. Long, *Science*, 2012, **335**, 1606−1610.

22. Y. He, R. Krishna and B. Chen, *Energy Environ. Sci.*, 2012, **5**, 9107−9120.

23. H. S. Scott, M. Shivanna, A. Bajpai, D. G. Madden, K.-J. Chen, T. Pham, K. A. Forrest, A. Hogan, B. Space and J. J. Perry IV, *ACS Appl. Mater. Inter*., 2017, **9**, 33395−33400.

24. P. Li, Y. He, Y. Zhao, L. Weng, H. Wang, R. Krishna, H. Wu, W. Zhou, M. O'Keeffe, Y. Han and B. Chen, *Angew. Chem. Int. Ed*., 2015, **54**, 574−577.

25. R. B. Lin, L. Li, H. Wu, H. Arman, B. Li, R. G. Lin, W. Zhou and B. Chen, *J. Am. Chem. Soc*., 2017, **139**, 8022−8028.

26. J. Gao, X. Qian, R. B. Lin, R. Krishna, H. Wu, W. Zhou and B. Chen, *Angew. Chem. Int. Ed*., 2020, **59**, 4396−4400.

27. W. Fan, S. Yuan, W. Wang, L. Feng, X. Liu, X. Zhang, X. Wang, Z. Kang, F. Dai, D. Yuan, D. Sun and H. C. Zhou, *J. Am. Chem. Soc*., 2020, **142**, 8728−8737.

28. L. Liu, Z. Yao, Y. Ye, Y. Yang, Q. Lin, Z. Zhang, M. O'Keeffe and S. Xiang, *J. Am. Chem. Soc.*, 2020, **142**, 9258−9266.

29. H. Zeng, M. Xie, Y. L. Huang, Y. Zhao, X. J. Xie, J. P. Bai, M. Y. Wan, R. Krishna, W. Lu and D. Li, *Angew. Chem. Int. Ed.*, 2019, **58**, 8515−8519.

30. J. Pei, K. Shao, J. X. Wang, H. M. Wen, Y. Yang, Y. Cui, R. Krishna, B. Li and G. Qian, *Adv. Mater.*, 2020, **32**, e1908275.

31. Z. Niu, X. Cui, T. Pham, G. Verma, P. C. Lan, C. Shan, H. Xing, K. A. Forrest, S. Suepaul, B. Space, A. Nafady, A. M. Al-Enizi and S. Ma, *Angew. Chem. Int. Ed*.,

2021, **60**, 5283−5288.

32. X. Rao, J. Cai, J. Yu, Y. He, C. Wu, W. Zhou, T. Yildirim, B. Chen and G. Qian, *Chem. Commun*., 2013, **49**, 6719−6721.

33. Y. He, R. Krishna and B. Chen, *Energy Environ. Sci*., 2012, **5**, 9107−9120.

34. J. Pang, F. Jiang, M. Wu, C. Liu, K. Su, W. Lu, D. Yuan and M. Hong, *Nat. Commun*., 2015, **6**, 7575.

35. J. Duan, W. Jin and R. Krishna, *lnorg. Chem*., 2015, **54**, 4279−4284.

36. H. S. Scott, M. Shivanna, A. Bajpai, D. G. Madden, K. J. Chen, T. Pham, K. A. Forrest, A. Hogan, B. Space, J. J. Perry Iv and M. J. Zaworotko, *ACS Appl. Mater. Inter*., 2017, **9**, 33395−33400.